Nanoscale

Semiconducting α'−boron sheet with high mobility and low all-boron contact resistance: A first-principles study

Journal:	*Nanoscale*
Manuscript ID	NR-ART-01-2021-000329.R1
Article Type:	Paper
Date Submitted by the Author:	19-Mar-2021

Complete List of Authors:	Zhang, Jun-Jie; Rice University, Altalhi, Tariq; Taif University, Chemistry Yang, Jihui; Rice University Yakobson, Boris; Rice University

SCHOLARONE™
Manuscripts

Semiconducting α'−boron sheet with high mobility and low all-boron contact resistance: A first-principles study

Jun-Jie Zhang[1], *Tariq Altalhi*[2], *Ji-Hui Yang*[1]*, *and Boris I. Yakobson*[2,3]*

[1]Department of Material Science & NanoEngineering, Rice University, Houston, Texas 77005, United States

[2]Chemistry Department, Taif University, Taif, Saudi Arabia

[3]Department of Chemistry, Rice University, Houston, Texas 77005, United States

Email: jhyang04@fudan.edu.cn; biy@rice.edu

Abstract

Two-dimensional field effect transistors (2D FETs) with high mobility semiconducting channels and low contact resistance between the semiconducting channel and the metallic electrodes are highly sought components of future electronics. Recently, 2D boron sheets (borophene) offer a great platform for realizing ideal 2D FETs but stable semiconducting phases still remain much unexplored. Herein, based on first-principles calculations and tight-binding model, we first clarify that α'−boron is the most stable semiconductor phase of boron sheets, while reveal the mechanism of metal-to-semiconductor transition from α− to α'−boron. Then we demonstrate that the carrier mobility in α′− and metastable β_3^S −boron should be very high, due to small effective masses of electrons and holes, as a good candidate material for 2D FETs. Considering further the lateral contacts between semiconducting α′ and metallic borophene, we find that the α′− and β_3^S −boron sheet can form Ohmic contacts with selected metallic boron sheets, without Schottky barrier. The high energetic stability and excellent mobility properties of α′−boron sheet together with its good contact match to metallic borophene electrodes are promising for fully boron-based FETs in the real 2D atomically thin limit.

1. INTRODUCTION

Field effect transistors (FETs) based on 2D materials have attracted intense interest because they show promise for short-channel FETs. Compared to the 3D case, electrons in 2D materials are confined in naturally atomically thin channels and, hence, all carriers are uniformly influenced by the gate voltage, which allows the suppression of current leakage.[1] In general, the performance of 2D FETs is determined by the semiconducting channel material and the contact resistance between the semiconducting channel and the metallic electrodes. The channel materials require 2D semiconductors with high carrier mobility (permitting the fast switching speed) and of sizable bandgaps (to ensure high on/off ratio); this rules out graphene for FET applications because of its absence of gap, despite the extremely high mobility due to its linear band dispersion near the Dirac points. Currently, the predominant channel materials for 2D FETs are phosphorene and transition metal dichalcogenides (TMDs) such as MoS_2.[2-4] While the former often suffers serious stability issue, the latter has relatively low carrier mobility.[5] Consequently, novel FET channel materials are still desired. Besides the intrinsic properties of channel materials, the contact issue between the channels and the electrodes is another challenging problem for 2D short-channel FETs. To reach the ballistic limits in scaled FETs for energy-efficient logic switching,[1] the contact resistance must be below certain values, i.e., forming Ohmic contact. The commonly existing Schottky barrier between 2D channels and metallic electrodes must be reduced. For this purpose, strategies like using heavily doped multilayers as contacts and using selective electrodes such as scandium for MoS_2 FETs have been proposed with limited success. Recently, phase engineering shows promise to reduce the contact resistance between the 2D channels and electrodes by forming their lateral heterostructures. For example, contact resistance in semiconducting 2H-MoS_2 FETs is impressively decreased when using metallic 1T-MoS_2 as the electrode, mainly due to the atomically sharp interface and lower Schottky barrier between the phases.[3, 6] Besides, phase

engineering in $MoTe_2$ by laser irradiation has been shown to fabricate Ohmic contacts.[7]

While phase engineering strategy offers a promising route for building 2D FETs based on lateral heterostructures with low contact resistance, it requires a 2D material to have both semiconducting and metallic phases, with similar lattices, for forming lateral heterostructures with sharp interfaces.[8] Recently, boron sheets are proposed to be ideal systems for the ideal 2D FETs.[9] Boron (B), on the left of carbon in the periodic table, is one of the most mysterious elements due to its multicenter chemical bond, exhibiting diverse 2D structures.[10] Unlike graphene, the honeycomb structure of boron sheet is difficult to be stabilized since boron lacks one electron to maintain sp^2 hybridization.[11-12] Derived from B_{80} fullerene,[13] the triangular sheet with various hollow hexagons is more favorable for boron sheet,[14-17] resulting in various chemical and physical properties. Until now, most of 2D boron are concluded to be metallic,[14-16, 18-19] whereas a few particular structures reveal semiconducting characteristic,[16, 20] such as α′,[16] β_3^S,[20] antiferromagnetic borophenes (AFM-B),[21] and $B_{12\text{-}1}$,[9] *et. al.* While the polymorphism of 2D boron sheets might hold great potential for the above-mentioned phase-engineering 2D FETs, the realization of real devices relies on the successful fabrication of various boron phases. So far, the experimentally synthesized boron sheets are all triangle-lattice-based metallic boron sheets and they generally have much lower total energies than most of the proposed semiconducting boron phases except the α′ phase which not only has small total energies compared to the metallic phases but also has similar triangle lattices, making it very promising for the channel of boron FETs. However, depending on the computational functionals, α′ phase appears either metallic or semiconducting. Therefore, to make boron-sheet-based 2D FETs come true, it is very important to clarify the stability, electronic, transport and contact properties of α′ boron sheet.

In this work, we perform first-principles and tight binding (TB) model calculations to analyze the electronic and transport properties of α′−boron sheet. First, the electronic structures of two

of the most energetically stable boron sheets, α-boron[14] and α′-boron[16], are verified by hybrid Heyd-Scuseria-Ernzerhof (HSE06) functional and GW0 approximations to resolve the previous controversies.[14-16] We demonstrate α′-boron is semiconducting (and dynamically stable), while α-boron is metallic (but was found to display soft phonon mode suggesting possible dynamic instability)[16]. TB model is adopted to give deeper insight into the electronic difference between them, revealing that the metal-semiconductor transition from α-boron to α′-boron is due to hybridization between π-bond and $s+p_{x,y}$ orbitals caused by the structure buckling. Furthermore, α′-boron is found to have high electron mobility (~ 20,000 $cm^2V^{-1}s^{-1}$) because the conduction-band minimum (CBM) is dominated by a π bond, similar to graphene. Besides α′-boron, another semiconducting β_3^S-boron sheet predicted by Xu *et. al*[20] with a triangle-lattice and higher energy is also considered as 2D FET channel, with relatively high carrier mobility as well. To choose appropriate contact electrodes which can form Ohmic contact with the above two semiconductors, in order to design the fully boron-sheet-based 2D FETs, the work functions of various metallic 2D boron phases are studied. Our results show that semiconducting 2D boron channels can form Ohmic contact with boron metallic phases, i.e. $B_{1/27}$ (derived from B_{36} cluster)[22] and $B_{1/10}$ sheets can form Ohmic contact with α′-boron sheet and $B_{1/10}$ and χ_3 sheets can form Ohmic contact with β_3^S-boron sheet. Our study will be helpful for the design of all-monoelemenal 2D FETs from semiconducting and metallic boron sheets.

2. COMPUTATIONAL METHODS

The density functional theory (DFT) calculations have been performed using the Vienna *ab initio* Simulation Package (VASP).[23-24] The projector-augmented wave (PAW) potentials with the generalized gradient approximation of Perdew-Burke-Ernzerhof (GGA-PBE) formulation are used with a cut-off energy 500 eV. The selected 2D Brillouin zones, sampled in the Monkhorst-Pack scheme, are determined by performing extensive convergence analyses (the

change of energy is less than 10^{-5} eV). A vacuum layer with 15 Å thickness is introduced to eliminate interaction between layers. To obtain accurate electronic structure of α- and α′-boron, hybrid HSE06 functional and partially self-consistent GW0 calculations are employed.[25-26] The standard exact-exchange mixing parameter α of 0.25 is used for the HSE06 functional.

3. RESULTS AND DISCUSSIONS

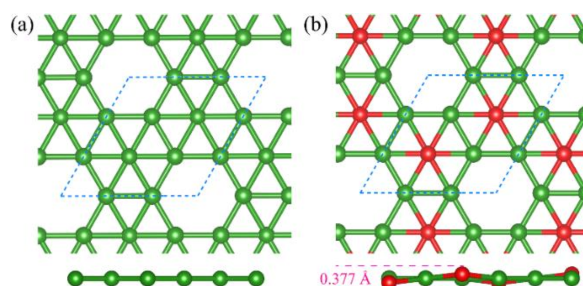

Figure 1. Top and side views of structures for (a) α- and (b) α′-boron sheets. Red denotes boron atoms moved off the plane. The blue dashed line indicates the selected unit cell.

α-boron sheet (Figure 1(a)), derived by unfolding B_{80} fullerene into 2D forms, is found to be one of most stable 2D boron sheets.[14-15] It is composed of triangular lattice patterned by isolated hollow hexagons, with a D_{6h} symmetry. However, Wu *et. al* found α-boron is dynamic unstable due to some negative frequencies in the out-plane atomistic ZA mode, implying that it will transform into slightly buckled α′-boron (Figure 1(b)),[16] having lower energy than α phase. In α′-boron sheet, the boron atoms that have 6 bonds with neighbors are shifted off the plane in alternating directions (Figure 1(b)), reducing the symmetry to D_{3d}.

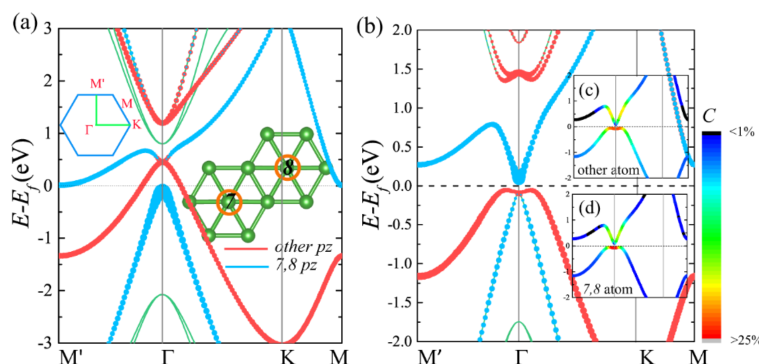

Figure 2. The band structures of (a) α- and (b) α′-boron sheet. Blue lines are projected p_z orbitals of six-bonding boron atoms and red lines denote projected p_z orbitals of five-bonding

boron atoms. The insets (c) and (d) are projected s, p_x, p_y orbitals of 6- and 5-bonding boron atoms, respectively. The color map represents their contributions.

Different from previous result that α-boron is semiconducting based on hybrid PBE0 calculation,[16] HSE06 (Figure 2(a)) and more accurate GW0 (see supporting information Figure S1(a)) calculations reconfirm α-boron as a metal, whereas α′ phase is a semiconductor with an indirect band gap of ~ 0.25 eV (according to more precise GW0 calculation, Figure S1(b)), but visibly smaller (~ 0.12 eV) in Figure 2(b) obtained with HSE06 functional. Since the HSE06 functional gives overall dispersion curves similar to GW0 (Figure 2 and Figure S1), our following calculations employ the HSE06. Based on the projected band structure, the states around the Fermi level are dominantly contributed by p_z orbitals in α- and α′-boron (Figure 2), which is similar to graphene. Then, the TB model including the p_z orbitals is adopted to gain further insight into the difference between them. The Hamiltonian with nearest neighbour (NN) hopping is as following,

$$H = H_0 + H_{NN} \quad (1)$$

where H_0 and H_{NN} are on-site energy and NN hopping, respectively. They read

$$H_0 = \sum_{L,\alpha} \varepsilon_{L\alpha} C^{\dagger}_{L\alpha} C_{L\alpha},$$
$$H_{NN} = -\sum_{\alpha,\beta} t_{\alpha\beta} C^{\dagger}_{\beta} C_{\alpha},$$

where $C_{L\alpha}$ and $C^{\dagger}_{L\alpha}$ represent the electron creation and annihilation operators at site α of sublattice L, respectively. $t_{\alpha\beta}$ is the hopping integral from site α to nearest neighbour site β, where $\beta = \alpha + \delta$. After considering the symmetry of α-boron, the hopping integrals can be divided into three groups (see Figure 3(a)): t_1 - between two different hollow hexagons (e.g. atom 1 to 2), t_2 - between hexagonal center and edge (e.g. atom 1 to 8), and t_3 - between same hollow hexagons (e.g. atom 1 and 4), respectively. The on-site energy has two groups: the on-site energy of the atoms with five bonds (ε_1) and that of atoms with six bonds (ε_2). Therefore, the total Hamiltonian in reciprocal space is summarized as following,

$$H = \frac{1}{N}\sum_{l}\varepsilon_l C_{k_l}^{\dagger} C_{k_l} + \frac{1}{N}\sum_{lm} t_{lm}(e^{-i\delta} C_{k_l}^{\dagger} C_{k_m} + e^{i\delta} C_{k_m}^{\dagger} C_{k_l}). \quad (2)$$

The eight-band TB model is employed to fit the band structure according to the HSE06 results (Table 1). By comparing the model bands with HSE06 bands, we can see that they agree well with each other except in some small regions (Figure S3(a)). The obtained values for on-site energy ε_1 and ε_2 are -1.90 and -2.65 eV, respectively, indicating lower p_z orbitals energy in sixfold-bonded atoms. Thus, the metallic properties of α-boron are fully caused by unsaturated π bonding of five-bonded atoms, which is in good agreement with projected HSE06 results (Figure 2(a)).

Table 1. Fitted TB model parameters (eV) to match HSE06 results in α-boron sheet.

	t_1	t_2	t_3	ε_1	ε_2
α-boron	2.55	2.05	2.19	-1.90	-2.65

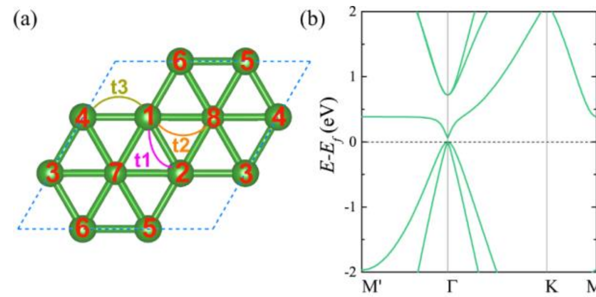

Figure 3. (a) Sketched electron hopping between nearest-neighbor atoms. (b) TB model results with t_2=1.6 eV, ε_2=-2.2 eV. The band structure opens a gap.

In α′-boron sheet, due to lack of mirror symmetry, p_z states are slightly coupled to p_x and p_y states, as well as s states (Figure 2(c-d)), leading to the opening of a band gap around Γ point. Unlike α-boron sheet, the π-bond between hexagonal center and edge is disturbed by s and $p_{x,y}$ orbitals, which have effects on the on-site energy of six-fold bonded atoms as well as the hopping energy between six- and five-fold bonded atoms. Accordingly, we change the values

of t_2 and ε_2 to 1.6 and -2.2 eV, respectively, in the α-boron sheet TB model. As expected, these lead to metal-semiconductor transition in the system (Figure 3(b)), which is consistent with HSE06 results. If one continuously decreases the values of t_2 to 1.4 eV and increases ε_2 to -2.0 eV, the corresponding band gap becomes larger (Figure S3(b)). Therefore, we conclude that semiconducting properties of α′-boron sheet are mainly caused by the hybridization between π-bond and s+$p_{x,y}$ orbitals.

Table 2. Total energies (eV/atom) of semiconducting α′-boron sheet in comparison with previous semiconducting boron sheet.

	α′	β^s_3 (ref.[20])	B_8-1 (ref.[9])	B_{12}-1□□ (ref.[9])	AFM-B (ref.[21])
E	-6.282	-6.202	-6.207	-6.208	-6.162

After confirming the semiconducting properties of α′-boron sheet, we then compare its total energy with other semiconducting boron phases. As seen in Table 2, α′-boron sheet is the most stable one among the semiconducting boron sheets. Considering its similar lattice with those metallic phases, we expect the most experimental feasibility of α′-boron sheet.

Because π-bonding plays a predominant role near the Fermi surface, quasi-linear dispersion is found near the CBM at Γ point, indicating much smaller effective electron masses and thus promising electron mobility. To calculate the carrier effective masses, the parabolic approximation for the band structure near the band edges is employed,

$$E_i(k) = \frac{\hbar^2}{2m_i^*}k^2 \tag{3}$$

where the effective mass m_i^* is m_h^* for holes and m_e for electrons. As expected, the electron effective mass (only ~0.05 m_0) in α′-boron is strikingly an order of magnitude smaller than typical values, i.e. 0.14 m_0 for monolayer black phosphorus,[27] and 0.45 m_0 for monolayer MoS_2.[28] For the holes, the flat dispersion around the VBM leads to a larger value, which, however, is still relatively small (~0.36 m_0). To estimate the carrier mobility of α′-boron, the

phonon-limited scattering model is used considering two orthogonal directions Γ-M' (x) and Γ-K (y) as indicated in Figure 2. The formula is, [5, 27, 29-30]

$$\mu = \frac{e\hbar^3 C}{k_B T m_i^* m_d (E_1^i)^2} \quad (4)$$

where m_d is the carrier average effective mass determined by $m_d = \sqrt{m_e^* m_h^*}$. E_1 is deformation potential constant of the VBM for hole or the CBM for electron along the transport direction, defined by $E_1^i = \Delta E_i / (\Delta l / l_0)$, where ΔE_i is the energy shift of VBM/CBM with respect to the lattice dilation/compression from the equilibrium distance l_0 by a distance of Δl along the transport direction. The elastic modulus term C is obtained following the expression as $(E-E_0)/S_0=C(\Delta l/l_0)$, where S_0 is the lateral area of the equilibrium cell, and E_0 and E are the total energies of the equilibrium cell and dilated/compressed cells, respectively. To fit the value of C and E_1, we perform total energy calculations for different $\Delta l/l_0$ in the range of -0.5% to +0.5% along the x or y direction. These quantities are calculated using HSE06 functional and the corresponding data are presented in Table 3. Note that, the larger values of C in α′-boron indicate the stronger bonding between boron atoms. As expected, our predicted mobility for α′-boron has very large values for electrons (~2×10^4 $cm^2V^{-1}s^{-1}$ compared to ~10^3 for monolayer black phosphorus[2]) and significant values for holes (~1500 $cm^2V^{-1}s^{-1}$) as well. Besides, we find the mobility is nearly isotropic, almost identical along different directions for both electrons and holes. The asymmetric behaviors for electron and hole mobility can be understood from the π-bonding in α′-boron. In detail, the predominant contributions of π-bond in the CBM, combined with stronger conjugated effect, are more favorable for transport properties. However, the s+$p_{x,y}$ orbitals are involved to couple with p_z orbitals in the VBM (Figure 2(c-d)), which destroys the conjugated effect between π-bond. In addition, the value of E_1 for holes is somewhat larger than that of electrons, also indicating wavefunctions of p_z orbitals have more overlap between s+$p_{x,y}$ orbitals.

Table 3. Calculated carrier effective masses (in unite of m_0), deformation potentials (eV), elastic moduli (Jm^{-2}), and carrier mobilities (cm^{2}V^{-1}s^{-1}) along Γ-M' (x) and Γ-K (y) for α′-boron at 300 K.

	m_x*	m_y*	E_{1x}	E_{1y}	C_x	C_y	μ_x	μ_y
electron	0.052	0.053	3.890	3.759	184.75	187.26	21148	21377
hole	0.368	0.367	4.337	4.920	184.75	187.26	1928	1519

Alternatively, the carrier mobility μ can also be estimated using the Boltzmann transport theory, which is expressed as $\mu=\sigma / ne$,[5, 31] where σ donates the carrier conductivity, n is the carrier density, and e is the elementary charge. The value of σ can be calculated using Boltzmann method implemented in Wannier90 with a constant carrier relaxation time τ[31] while n can be easily calculated from DFT using the following expressions,[32]

$$n_0 = e^{-\frac{E_g - E_f}{k_B T}} \int_{E_g}^{\infty} d\varepsilon \left[1 + e^{-\frac{\varepsilon - E_f}{k_B T}}\right]^{-1} D(\varepsilon) \text{ (for electron density)}, \quad (5)$$

$$p_0 = e^{-\frac{E_f}{k_B T}} \int_{-\infty}^{0} d\varepsilon \left[1 + e^{-\frac{-\varepsilon}{k_B T}}\right]^{-1} D(\varepsilon) \quad \text{(for hole density)}, \quad (6)$$

where D(ε) represents the density of states with zero energy set at the VBM, E_f is the Fermi level, and E_g is band gap. Both σ and n are functions of electron chemical potentials or Fermi levels. Here, the carrier relaxation time is fitted as around 90 fs to match the value of electron or hole mobility, which is similar to previous works for phosphorene[5, 30] and the obtained results are shown in Figure S4. As we can see, both the hole and electron mobility are isotropic along the x and y directions, and electron mobility is about an order magnitude higher than hole mobility, in good agreement with the results obtained using the phonon-limited scattering model. However, this method doesn't require the dilation or compression of the equilibrium cells to obtain C and E_1 and also doesn't need to find two orthogonal directions, which is computationally cheaper and convenient. We apply this method to another semiconducting β_3^S

boron (Figure 4(a)) along the two directions defined in Figure 4(b) by assuming the same relaxation time, which is reasonable as both α′-boron and β_3^S boron sheets have similar boron triangle lattices. β_3^S boron has a direct band gap of 0.42 eV near Y-point, shown in Figure S5. Different from α′-boron, β_3^S boron has relatively large and anisotropic carrier mobility, i.e., the hole mobility (about 9×10^3 $cm^2V^{-1}s^{-1}$) in Y-Γ direction (denoted as *y* direction) is higher than that (about 6×10^3 $cm^2V^{-1}s^{-1}$) in Y-M direction (denoted as *x* direction), whereas the electron mobility in Y-M direction (~1.45×10^4 $cm^2V^{-1}s^{-1}$) is larger than Y-Γ direction (~7×10^3 $cm^2V^{-1}s^{-1}$). Besides, the carrier mobility along the Y-M direction shows asymmetric behavior for electrons and holes, that is, the electrons are being more mobile similar to the case in the α′-boron. In general, the carrier mobility is largely (although not solely) determined by their effective masses, which for the β_3^S boron can be calculated based on parabolic approximation above, yielding for the hole (electron) 0.24 m_0 (0.14 m_0) in Y-M direction, and 0.19 m_0 (0.21 m_0) in Γ-Y direction, which explains the above obtained respective carrier mobilities and anisotropic electronic transport behaviors in β_3^S boron. By comparing the mobility results of α′ and β_3^S boron, we conclude that α′-boron is more favorable for *n*-type FETs and β_3^S boron is more favorable for *p*-type FETs.

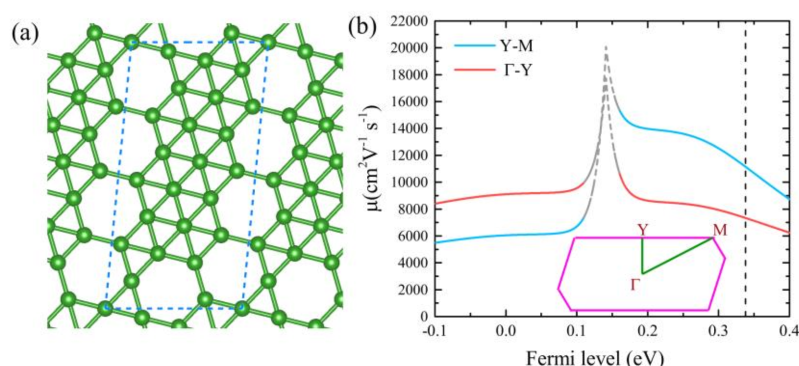

Figure 4. (a) Top view of β_3^S boron sheet. The blue dashed line indicates the selected unit cell. (b) Carrier mobility in β_3^S boron sheet calculated using $\mu=\sigma/ne$. The VBM is set as zero, while CBM is marked by the vertical dashed line. The plateaus above the VBM stand for the

hole mobility while the plateaus below the CBM stand for the electron mobility. The pink polygon denotes its Brillouin zone, with high symmetry points. Note that the peaks near the middle of bandgaps are caused by the too small carrier densities, which amplify any computational errors in σ, making results not very reliable and therefore indicated by dashed gray lines.

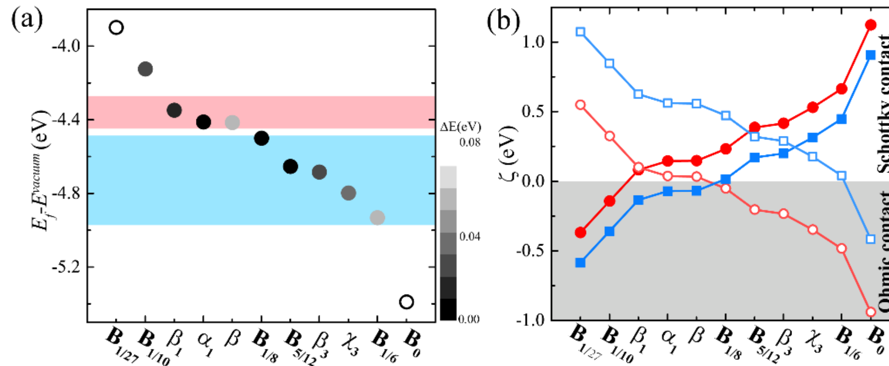

Figure 5. (a) Fermi level positions of various metallic boron sheets denoted as circles with respect to the vacuum level, which is set as zero (structures are shown in Supporting Information Figure S6). The VBM and CBM positions and the band gaps in semiconducting α′ - (red) and β_3^S - (blue) boron sheets are also shown. Color map and gray-level circles indicate the formation energy difference between $B_{1/8}$ and various metallic boron sheets. (b) The height of Schottky barrier ζ between n/p-type semiconducting and various metallic boron sheets. Red solid (hollow) circles indicate n-type (p-type) α′ boron sheets. Blue solid (hollow) squares indicate β_3^S n-type (p-type) boron sheets. Gray region indicates the formation of Ohmic contacts.

After demonstrating that the α′ and β_3^S layers are semiconductors with high carrier mobility, we now turn to the contacts between these two semiconducting boron phases and other well-known metallic phases. The contact resistance is known as a major challenge for 2D FETs, owing to the formation of a Schottky barrier between metallic electrode and semiconducting channel. Thus, the performance of FETs strongly depends on the choice of metallic electrode. Fortunately, boron itself provides various 2D metallic phases to serve as electrodes of semiconducting boron sheets. Here, several stable metallic phases are selected to calculate their work functions based on HSE06 functionals. The obtained Fermi level positions for metallic

boron sheets are shown in Figure 5(a), along with the CBM and VBM positions for α′ and β_3^S boron. Since the Anderson rule must hold for lateral junctions, and in accord to the theoretical investigation in Zhang *et. al*,[33] the height of barrier ζ for metal-semiconductor junction is defined by Schottky-Mott rule as $\zeta_n=\varphi-\chi$ for *n*-type semiconducting channels and $\zeta_p=\chi+E_g-\varphi$ for *p*-type semiconducting channels, where χ is electron affinity of semiconducting channels, and φ is work function of metallic boron sheets. The values of ζ for *n*- and *p*-type semiconducting boron sheet channels using different boron metallic electrodes are summarized in Figure 5(b), in which the zero or negative ζ represents the Ohmic contacts. As we can see, the Fermi level positions of some metallic boron sheets are outside the band gaps of α′ and β_3^S boron sheets. Consequently, the Ohmic contacts can be formed between metallic boron sheet and α′ and β_3^S boron sheets, which is highly desired for 2D FETs. For example, $B_{1/27}$ and $B_{1/10}$ sheets are favorable to form Ohmic contacts with α′-boron for *n*-type FETs, while more options can be chosen for the *p*-type semiconducting channels, such as $B_{1/8}$, $B_{5/12}$, $B_{1/6}$, and even triangular boron sheets. More importantly, all the boron sheets considered here share the same triangle boron lattice, while differ merely in B-vacancy distribution, ensuring the good metal-semiconductor lateral interfaces, and suggesting the possibility of fully boron-based atomically thin FETs, Figure 6. Besides, a large number of 2D boron FETs can be easily integrated on one large piece of boron sheet by making different patterns, paving the way to large scale integrated circuits.

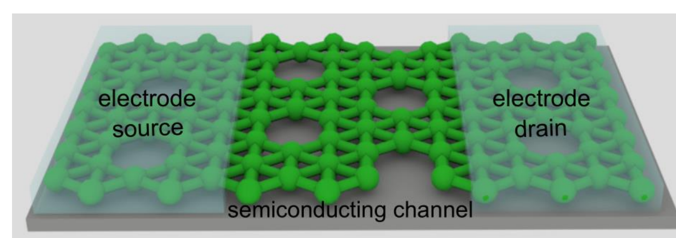

Figure 6. Sketched fully boron-based atom-thin FETs device. The electrodes consist of metallic boron sheets, and the semiconducting channel is α′ (shown) or β_3^S -boron sheet.

4. CONCLUSION

In summary, based on first-principles calculations and TB model, we have first clarified that α boron sheet is a metal, whereas α′ boron is a semiconductor with a finite band gap. The metal-to-semiconductor transition from α− to α′−boron sheet is attributed to the disturbance of π bonding by s, p_x, and p_y orbitals, in α′−boron sheet. We then demonstrate the semiconducting α′−boron sheet has very high carrier mobility due to its small carrier effective masses. Similar high carrier mobility is also demonstrated in another newly reported semiconducting β_3^S boron sheet, indicating these semiconducting boron sheets can be good channel materials for 2D FETs. We further consider the lateral contacts between semiconducting and metallic boron sheets. We found that both α′− and β_3^S boron sheets can form Ohmic contacts with selected metallic boron sheets without Schottky barriers. The excellent mobility properties of semiconducting boron sheets together with their good contact properties with metallic boron sheet electrodes, thus indicate that they can be very promising candidates for fully boron-sheet-based FETs in the real 2D atomically thin limits.

ASSOCIATED CONTENT

Supporting Information

GW0 results for α- and α′-boron sheet; More TB model results for α- and α′-boron; More carrier mobility results for α′- and β^S_3 boron sheet; Sketched structures of selected metallic boron sheet.

AUTHOR INFORMATION

Corresponding Author

jhyang04@fudan.edu.cn;biy@rice.edu

Notes

The authors declare no competing financial interests.

ACKNOWLEDGMENT

This work was supported by the Office of Naval Research, grant N00014-19-1-2191, and by Taif University Research Support Project (TURSP-HC2021/1, Saudi Arabia). Computations were performed on the NOTS HPC cluster running on the Rice University Big Research Data (BiRD) cloud infrastructure.

REFERENCES

1. Chhowalla, M.; Jena, D.; Zhang, H., Two-dimensional semiconductors for transistors. *Nat. Rev. Mater.* **2016,** *1* (11), 16052.

2. Li, L.; Yu, Y.; Ye, G. J.; Ge, Q.; Ou, X.; Wu, H.; Feng, D.; Chen, X. H.; Zhang, Y., Black phosphorus field-effect transistors. *Nat. Nanotechnol.* **2014,** *9* (5), 372.

3. Kappera, R.; Voiry, D.; Yalcin, S. E.; Branch, B.; Gupta, G.; Mohite, A. D.; Chhowalla, M., Phase-engineered low-resistance contacts for ultrathin MoS_2 transistors. *Nat. Mater.* **2014,** *13* (12), 1128.

4. Zhang, Z.; Guo, W., Intrinsic metallic and semiconducting cubic boron nitride nanofilms. *Nano Lett.* **2012,** *12* (7), 3650-3655.

5. Yang, J.-H.; Zhang, Y.; Yin, W.-J.; Gong, X.; Yakobson, B. I.; Wei, S.-H., Two-dimensional SiS layers with promising electronic and optoelectronic properties: theoretical prediction. *Nano Lett.* **2016,** *16* (2), 1110-1117.

6. Fan, Z.-Q.; Jiang, X.-W.; Luo, J.-W.; Jiao, L.-Y.; Huang, R.; Li, S.-S.; Wang, L.-W., In-plane Schottky-barrier field-effect transistors based on 1T/2H heterojunctions of transition-metal dichalcogenides. *Phys. Rev. B* **2017,** *96* (16), 165402.

7. Cho, S.; Kim, S.; Kim, J. H.; Zhao, J.; Seok, J.; Keum, D. H.; Baik, J.; Choe, D.-H.; Chang, K.; Suenaga, K., Phase patterning for ohmic homojunction contact in $MoTe_2$. *Science* **2015,** *349* (6248), 625-628.

8. Zhang, Z.; Chen, C.; Guo, W., Magnetoelectric effect in graphene nanoribbons on substrates via electric bias control of exchange splitting. *Phys. Rev. Lett.* **2009,** *103* (18), 187204.

9. Zhang, Y.-L.; Yang, J.-H.; Xiang, H.; Gong, X.-G., Fully Boron-Sheet-Based Field Effect Transistors from First-Principles: Inverse Design of Semiconducting Boron Sheets. *J. Phys. Chem. Lett.* **2020,** *12*, 576-584.

10. Zhang, Z.; Penev, E. S.; Yakobson, B. I., Two-dimensional boron: structures, properties and applications. *Chem. Soc. Rev.* **2017,** *46* (22), 6746-6763.

11. Boustani, I.; Quandt, A.; Hernández, E.; Rubio, A., New boron based nanostructured materials. *J. Chem. Phys.* **1999,** *110* (6), 3176-3185.

12. Evans, M. H.; Joannopoulos, J.; Pantelides, S. T., Electronic and mechanical properties of planar and tubular boron structures. *Phys. Rev. B* **2005,** *72* (4), 045434.

13. Szwacki, N. G.; Sadrzadeh, A.; Yakobson, B. I., B 80 fullerene: an ab initio prediction of geometry, stability, and electronic structure. *Phys. Rev. Lett.* **2007,** *98* (16), 166804.

14. Tang, H.; Ismail-Beigi, S., Novel precursors for boron nanotubes: the competition of two-center and three-center bonding in boron sheets. *Phys. Rev. Lett.* **2007,** *99* (11), 115501.

15. Penev, E. S.; Bhowmick, S.; Sadrzadeh, A.; Yakobson, B. I., Polymorphism of two-

dimensional boron. *Nano Lett.* **2012,** *12* (5), 2441-2445.

16. Wu, X.; Dai, J.; Zhao, Y.; Zhuo, Z.; Yang, J.; Zeng, X. C., Two-dimensional boron monolayer sheets. *ACS Nano* **2012,** *6* (8), 7443-7453.

17. Zhang, Z.; Yang, Y.; Penev, E. S.; Yakobson, B. I., Elasticity, flexibility, and ideal strength of borophenes. *Adv. Funct. Mater.* **2017,** *27* (9), 1605059.

18. Zhang, Z.; Penev, E. S.; Yakobson, B. I., Two-dimensional materials: polyphony in B flat. *Nat. Chem.* **2016,** *8* (6), 525.

19. Penev, E. S.; Kutana, A.; Yakobson, B. I., Can two-dimensional boron superconduct? *Nano Lett.* **2016,** *16* (4), 2522-2526.

20. Xu, S.-G.; Li, X.-T.; Zhao, Y.-J.; Liao, J.-H.; Xu, W.-P.; Yang, X.-B.; Xu, H., Two-Dimensional Semiconducting Boron Monolayers. *J. Am. Chem. Soc.* **2017,** *139* (48), 17233-17236.

21. Zhu, M.-H.; Weng, X.-J.; Gao, G.; Dong, S.; Lin, L.-F.; Wang, W.-H.; Zhu, Q.; Oganov, A. R.; Dong, X.; Tian, Y., Magnetic borophenes from an evolutionary search. *Phys. Rev. B* **2019,** *99* (20), 205412.

22. Piazza, Z. A.; Hu, H.-S.; Li, W.-L.; Zhao, Y.-F.; Li, J.; Wang, L.-S., Planar hexagonal B 36 as a potential basis for extended single-atom layer boron sheets. *Nat. Commun.* **2014,** *5* (1), 1-6.

23. Kresse, G.; Furthmüller, J., Efficient iterative schemes for ab initio total-energy calculations using a plane-wave basis set. *Phys. Rev. B* **1996,** *54* (16), 11169.

24. Kresse, G.; Joubert, D., From ultrasoft pseudopotentials to the projector augmented-wave method. *Phys. Rev. B* **1999,** *59* (3), 1758.

25. Heyd, J.; Scuseria, G. E.; Ernzerhof, M., Hybrid functionals based on a screened Coulomb potential. *J. Chem. Phys.* **2003,** *118* (18), 8207-8215.

26. Shishkin, M.; Marsman, M.; Kresse, G., Accurate quasiparticle spectra from self-consistent GW calculations with vertex corrections. *Phys. Rev. Lett.* **2007,** *99* (24), 246403.

27. Qiao, J.; Kong, X.; Hu, Z.-X.; Yang, F.; Ji, W., High-mobility transport anisotropy and linear dichroism in few-layer black phosphorus. *Nat. Commun.* **2014,** *5*, 4475.

28. Yoon, Y.; Ganapathi, K.; Salahuddin, S., How good can monolayer MoS2 transistors be? *Nano Lett.* **2011,** *11* (9), 3768-3773.

29. Bruzzone, S.; Fiori, G., Ab-initio simulations of deformation potentials and electron mobility in chemically modified graphene and two-dimensional hexagonal boron-nitride. *Appl. Phys. Lett.* **2011,** *99* (22), 222108.

30. Fei, R.; Faghaninia, A.; Soklaski, R.; Yan, J.-A.; Lo, C.; Yang, L., Enhanced thermoelectric

efficiency via orthogonal electrical and thermal conductances in phosphorene. *Nano Lett.* **2014,** *14* (11), 6393-6399.

31. Pizzi, G.; Volja, D.; Kozinsky, B.; Fornari, M.; Marzari, N., BoltzWann: A code for the evaluation of thermoelectric and electronic transport properties with a maximally-localized Wannier functions basis. *Comput. Phys. Commun.* **2014,** *185* (1), 422-429.

32. Yang, J.-H.; Yin, W.-J.; Park, J.-S.; Wei, S.-H., Self-regulation of charged defect compensation and formation energy pinning in semiconductors. *Sci. Rep.* **2015,** *5*, 16977.

33. Zhang, J.; Xie, W.; Zhao, J.; Zhang, S., Band alignment of two-dimensional lateral heterostructures. *2D Mater.* **2016,** *4* (1), 015038.